

Flow behavior of polypropylene reactor powder in horizontal stirred bed reactors characterized by X-ray imaging

van der Sande, P. Christian; de Vries, Claris; Wagner, Evert C.; Vöglander, Amarenske C.; Meesters, Gabrie M.H.; van Ommen, J. Ruud

DOI

[10.1016/j.cej.2024.156891](https://doi.org/10.1016/j.cej.2024.156891)

Publication date

2024

Document Version

Final published version

Published in

Chemical Engineering Journal

Citation (APA)

van der Sande, P. C., de Vries, C., Wagner, E. C., Vöglander, A. C., Meesters, G. M. H., & van Ommen, J. R. (2024). Flow behavior of polypropylene reactor powder in horizontal stirred bed reactors characterized by X-ray imaging. *Chemical Engineering Journal*, 500, Article 156891. <https://doi.org/10.1016/j.cej.2024.156891>

Important note

To cite this publication, please use the final published version (if applicable). Please check the document version above.

Copyright

Other than for strictly personal use, it is not permitted to download, forward or distribute the text or part of it, without the consent of the author(s) and/or copyright holder(s), unless the work is under an open content license such as Creative Commons.

Takedown policy

Please contact us and provide details if you believe this document breaches copyrights. We will remove access to the work immediately and investigate your claim.



Flow behavior of polypropylene reactor powder in horizontal stirred bed reactors characterized by X-ray imaging

P. Christian van der Sande^{*}, Claris de Vries, Evert C. Wagner, Amarenske C. Vögtlander, Gabriele M.H. Meesters, J. Ruud van Ommen^{*}

Delft University of Technology, Department of Chemical Engineering, van der Maasweg 9, Delft, 2629HZ, The Netherlands

ARTICLE INFO

Keywords:

Horizontal stirred bed reactors
Polypropylene
X-ray
Multiphase reactors
Reactor optimization

ABSTRACT

Horizontal stirred bed reactors (HSBRs) are widely used in the commercial production of polypropylene (PP). Despite their commercial significance, a comprehensive understanding of the flow behavior in HSBRs remains elusive, primarily due to the lack of detailed experimental data. This study investigates the influence of operating parameters on the particle flow behavior of two types of PP reactor powder in a laboratory-scale HSBR using X-ray imaging. Our results indicate that the overall flow behavior and phase holdup in the HSBR are dominated by agitation. Moreover, gas injection through the inlet points at the bottom of the HSBR results in spouting behavior, which can lead to reduced gas–solid contacting and, in extreme cases, complete bypass. Finally, the presence of liquid (in this study, isopropyl alcohol) adversely affects the flow behavior of the PP reactor powder due to liquid bridging at the contact points of particles. Powders that comprise particles with relatively small sizes and dense surface morphology are particularly prone to reduced flow behavior when exposed to liquid.

1. Introduction

Polypropylene (PP) is a cost-effective and versatile polyolefin resin with good mechanical properties, thermal stability, and chemical resistance. These characteristics make PP a preferred choice in various industries, including food packaging, automotive, healthcare, textiles, and electronics [1,2]. In 2022, the annual global production of PP was approximately 79.1 million metric tons [3], and the global PP market is expected to see sustained growth, driven by the increased use of high-quality plastics in automotive manufacturing and the growing need for efficient packaging solutions [4].

Gas-phase catalyzed polymerization has become a crucial method in the commercial production of PP [5]. The Innovene™ PP process stands out as a particularly effective and scalable production technology [6–10]. This process typically employs two horizontal stirred bed reactors (HSBRs): the first reactor is used for forming propylene homopolymer or random copolymer, and the second downstream reactor is dedicated to producing propylene impact copolymer. HSBRs are highly valued for their ability to provide excellent gas-phase mixing and precise control over reaction parameters, which are essential for efficient PP production.

The HSBR is a cylindrical reactor comprising a series of paddles attached to a central shaft. A schematic representation of the HSBR

is depicted in Fig. 1. At the reactor's inlet, micron-sized Ziegler–Natta catalyst particles are continuously introduced [10]. Gaseous propylene monomers are injected through inlets at the reactor's base and polymerize on the active sites of the catalyst through a coordination-insertion mechanism. To maintain a sub-fluidized state and prevent bed fluidization, the gas velocity is carefully regulated. Heat originating from the highly exothermic polymerization reaction is removed through evaporative cooling. This process involves spraying recycled liquid propylene onto the PP powder bed from various axial positions along the reactor's length. When the liquid propylene contacts the active PP, it vaporizes, absorbing the reaction heat and thereby cooling the system effectively. Throughout the polymerization process, the mildly agitated PP powder is kept at a constant inventory, allowing the PP particles to grow to sizes between 100 and 5000 μm [11]. The increasing volume of the growing particles propels the powder toward the reactor's opposite end, where it is continuously discharged.

There are significant operational challenges involved in gas-phase polymerization reactors that often arise from inadequate particle movement or insufficient cooling. A primary concern is the agglomeration of polyolefin particles, which can reduce production capacity and product quality [12,13]. In the Innovene™ PP process, such agglomeration is typically due to insufficient heat dissipation from inadequate quenching

^{*} Corresponding authors.

E-mail addresses: P.C.vanderSande@tudelft.nl (P.C. van der Sande), J.R.vanOmmen@tudelft.nl (J.R. van Ommen).

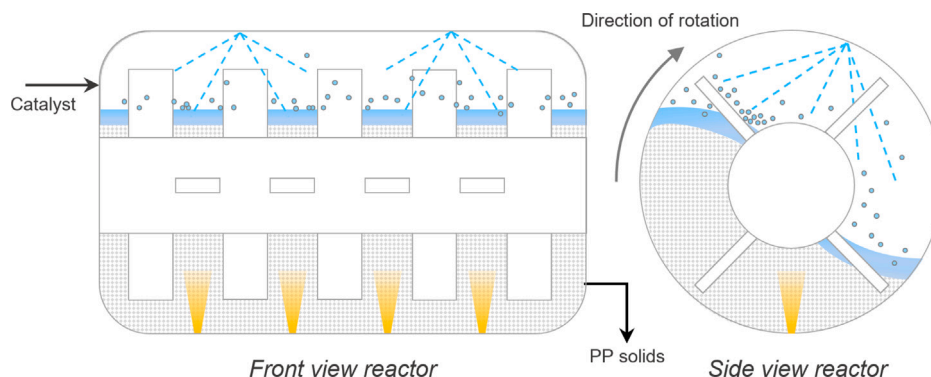


Fig. 1. Graphical representation of the front view (left) and side view (right) of the horizontal stirred bed reactor as employed in the Innovene™ PP process. The polypropylene solids are continuously agitated, while gaseous propylene is introduced from the bottom (yellow cones), and liquid propylene quench is sprayed from the top of the reactor (blue dashed lines).

or poor solids circulation. Without effective and uniform heat dissipation, the temperature of polymer particles can increase, potentially reaching or exceeding their softening or melting point, leading to the formation of agglomerates or lumps. These agglomerates reduce product quality and can obstruct the discharge pipeline, disrupt the heat exchange balance, and cause deviations from the normal flow pattern, significantly impairing reactor efficiency. In severe cases, agglomerates can occupy a large portion of the reactor volume, necessitating unscheduled plant shutdowns for cleaning and resulting in significant financial penalties [14].

While a propylene quench is necessary to dissipate heat and control the reactor temperature, excess liquid propylene can create liquid bridges between particles, increasing cohesion through capillary forces [15]. This liquid bridging may lead to the formation of liquid-bound PP agglomerates, which in turn deteriorates flowability. Therefore, it is crucial to determine the optimal liquid quench rate that effectively dissipates heat while minimizing adverse effects on PP flow behavior caused by liquid bridging. Additionally, adequate solids circulation is essential to ensure uniform wetting and maintain a consistent bed temperature.

Considerable research effort has been devoted to kinetic studies of the polymerization reaction and modeling of the residence time distribution [5,8–10,16–19]. The literature widely reports that the powder mixing pattern in an HSBR is influenced by two transport effects: simultaneous stirring flows with equal intensity in both the up- and downstream directions and the continuously increasing powder net flow in the downstream direction due to particle growth. Together, these effects give rise to a residence time distribution that can be effectively modeled by three to five continuous stirred tank reactors in series [8,17].

While considerable effort has been devoted to kinetic studies and modeling, only limited studies have explored the powder flow behavior in HSBRs. The flow characteristics of biomass particles in a laboratory-scale HSBR were examined through experimental measurements [20] and computational modeling [21]. These studies reported that the axial dispersion coefficient increases with higher rotation speeds and a larger number of blades.

Additionally, the granular flow pattern in horizontal powder mixers, which shows similarities to HSBRs, has been investigated using positron emission particle tracking [22–24]. Laurent et al. [22] observed that radial blades in horizontal mixers create axial compartments in the bed that induce circulation loops in the bed. Subsequent research by Laurent and Bridgwater [23] demonstrated that the velocity fields and axial dispersion coefficients scale with rotation speed, aligning with the flow characteristics observed in the HSBR study by Xi et al. [20]. Furthermore, Laurent and Bridgwater [24] reported that at sufficiently high reactor fill levels, the agitator shaft significantly influences radial and axial particle motion.

Experimental evaluation of the powder flow behavior and phase holdup is essential for optimizing and intensifying reactor operations and validating computational models. The flow pattern and phase holdup significantly affect reactor stability and the quality and uniformity of the final polymerized product. However, the complex hydrodynamics of multiphase flow reactors pose a challenge for experimental evaluation. In the HSBR, the flow's multiphase nature, characterized by a high particulate phase fraction, results in a dense, opaque flow that hinders the use of conventional optical techniques.

In our previous work, we characterized the particle dynamics in a laboratory-scale HSBR by employing single-photon emission radioactive particle tracking. We found that the particle dynamics are highly influenced by the reactor fill level and agitator rotation speed [25,26]. However, the particle tracking method employed did not allow for the study of the overall flow behavior and gas holdup.

In the current study, we characterize the flow behavior of two types of PP reactor powder in a laboratory-scale HSBR under non-reactive conditions, employing an in-house X-ray imaging method. X-ray imaging has been an established non-invasive technique for assessing the phase holdup in multiphase flow systems [27–31]. We employ X-ray imaging to investigate the influence of reactor operating parameters, namely agitator rotation speed, gas inlet flow rate, and liquid content, on the flow behavior and gas holdup in the HSBR. Furthermore, we employ in-house developed software to implement X-ray imaging phase-locking, enabling local assessment of the relation between the phase holdup and the power consumption by the motor driving the agitator.

2. Methodology

2.1. Horizontal stirred bed reactor setup

The laboratory-scale HSBR used in this work consists of a 134 mm inner-diameter cylinder with a length of 150 mm. The cylinder incorporates an agitator comprising a central shaft with seven blade positions. Each position is equipped with two blades, with each blade positioned 90° apart from its neighboring blades. The inner blades have a width of 20 mm, while the end blades have a width of 15 mm. The cylinder has three gas injection inlets of 6 mm diameter at the bottom at 25, 50, and 75% of the length. The injection points are equipped with a filter to prevent back-flow of solids. The two outlets are closed through a filter to prevent fines elutriation. Both the cylinder and the agitator are constructed from polycarbonate to mitigate X-ray radiation attenuation during the experiments. The agitator can be rotated at the desired rotation speed using an electric motor with a belt drive, which is controlled via in-house software. A schematic representation of the HSBR is illustrated in Fig. 2.

Table 1
Physical properties of the powders used in this study.

Powder	$d_{3,2}$ (μm)	$d_{4,3}$ (μm)	Span ^a (-)	ρ_{bulk} (kg m^{-3})	u_{mf} (cm s^{-1})	Shape
PP-1	569	672	1.12	511	15	Angular
PP-3	1040	1180	0.99	368	25	Spherical

$$^a \text{Span} = (d_{v90} - d_{v10}) / d_{v50}$$

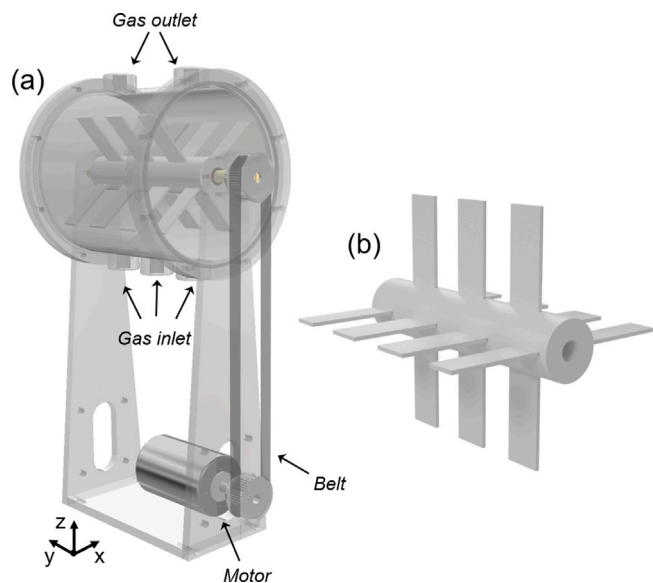


Fig. 2. Schematic representation of (a) the laboratory-scale horizontal stirred bed reactor and, (b) the internal agitator comprising a central shaft equipped with a series of impellers.

2.2. Polypropylene material

This study assesses the flow behavior of two types of industrial-grade PP reactor powder. It is important to note that these powders are PP solids directly acquired from industrial HSBRs and possess significantly different properties than processed PP beads, which are typically used in academic studies. The PP powders investigated were manufactured with different catalysts and consequently possess different inherent particle properties. For ease, the powders are denoted as PP-1 and PP-3. The particle size distribution and morphology of the powders were analyzed using a particle size analyzer and microscopy, respectively. The physical properties of the materials are summarized in Table 1 and will be further discussed in the following paragraphs.

The particle size distributions of the PP materials were measured using the Malvern 3000 particle size analyzer equipped with a dry powder module and high-energy stainless steel venturi tube. The volume-based particle size distributions are represented in Fig. 3(a). Among the two powders, PP-3 exhibits the largest particles with a Sauter mean particle size ($d_{3,2}$) of 1040 μm compared to 569 μm of PP-1. As can be observed from the cumulative distribution and the span denoted in Table 1, PP-1 has a slightly broader particle size distribution than PP-3.

The morphology of the materials was characterized through optical and scanning electron microscopy. A ZEISS SterEO Discovery.V8 optical microscope with manual 8x zoom was used to acquire images on the macro-scale. Fig. 3(b)(1-2) shows representative optical microscope images of the powders. The images illustrate notable variations in the size and shape of the particles, and both materials can be classified as poly-disperse in size and shape. In agreement with the particle size distribution obtained through light scattering, the images demonstrate that PP-3 exhibits the largest particles while PP-1 exhibits the smallest. Furthermore, the particles of PP-1 display angular morphology, while the particles of PP-3 possess a more spherical morphology. In addition,

a JEOL JSM-6010LA scanning electron microscope was used to acquire images at the micro-scale. Before the analysis, the samples were sputter-coated with gold using a JEOL JFC-1300 auto fine coater in automatic mode to limit charging and improve image quality. From the SEM images (Fig. 3(b)(3-4)), it can be observed that the surface of PP-1 is smooth and appears to be dense. In contrast, the surface of PP-3 demonstrates a higher degree of surface roughness and the presence of macro-pores. Additional SEM images are included in supplementary Appendix A.

Besides the particle size distribution and morphology, the loose bulk density (ρ_b) of the powders was experimentally determined following the method of Carr [32]. PP-1 has a relatively higher bulk density (511 kg m^{-3}) compared to PP-3 (368 kg m^{-3}). Moreover, the minimum fluidization velocity (u_{mf}) of the two powders was experimentally determined through pressure drop measurements in a cylindrical fluidized bed column with an internal diameter of 5 cm. The respective pressure drop against superficial gas velocity plots are included in the supplementary Fig. A.1. From the curves, the minimum fluidization velocities of PP-1 and PP-3 were determined to be 15 and 25 cm s^{-1} , respectively.

2.2.1. X-ray imaging

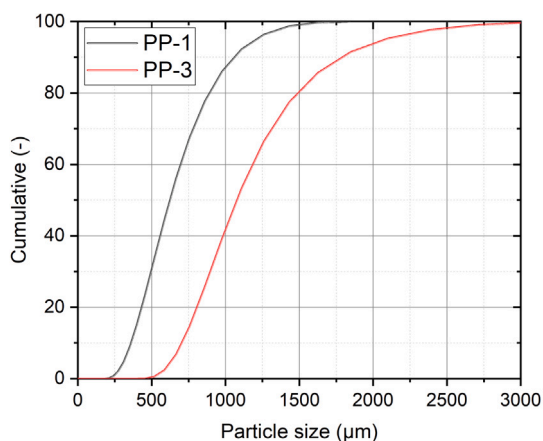
The flow behavior of the PP powders in the HSBR was experimentally assessed using an in-house fast X-ray imaging setup, schematically illustrated in Fig. 4(a). X-ray imaging is a non-invasive imaging technique that can be used to visualize the density distribution of opaque multiphase flows. With X-ray imaging, a 2D projection of the 3D gas holdup in the HSBR was captured.

The X-ray setup consists of a standard industrial-type X-ray source (Yxlon International GmbH) with a maximum energy of 150 keV working in cone beam mode and a 2D detector (Teledyne Dalsa Xineos) with a theoretical spatial resolution of 0.20 mm placed opposite of the source. In this study, the source-detector distance was 122.5 cm, with the center of the HSBR positioned 102 cm from the source. Throughout all experiments, the setup was controlled from a workstation located outside the setup room, ensuring a safe working environment. X-ray images were acquired at a sampling rate between 35 and 70 Hz depending on the desired resolution of the acquired image. The obtained data was then stored for subsequent digital image analysis.

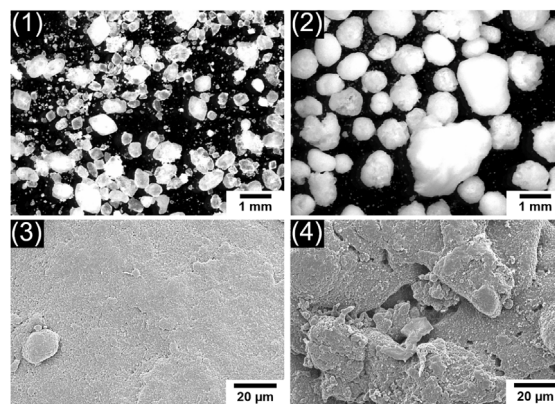
Each acquired image is a time-resolved projected 2D intensity map of the HSBR. A two-point calibration protocol was executed to convert the measurement intensity into a gas holdup (see Fig. 4(b)). Initially, a reference image was captured of the empty column without the shaft and impeller blades (I_{empty}). Subsequently, the column was filled with the bed material, and a full reference image was obtained (I_{full}). The X-ray measurement principle relies on the attenuation of X-rays traveling in a straight line from an X-ray source to a detector while passing through the material. The transmission of a monochromatic beam of high-energy photons with initial intensity I_0 through a material of constant density is described by the Lambert-Beer law:

$$I(x) = I_0 e^{-\mu x} \quad (1)$$

Here, $I(x)$ denotes the intensity measured at the detector, μ is the attenuation coefficient, and x is the thickness of the X-ray attenuating material between the source and the detector. In cases of varying attenuation, the measured intensity is the integral effect of local attenuation with the local attenuation coefficient. By applying the Lambert-Beer law, the measurement gas holdup map ($\epsilon_{g,\text{measurement}}$) was derived from

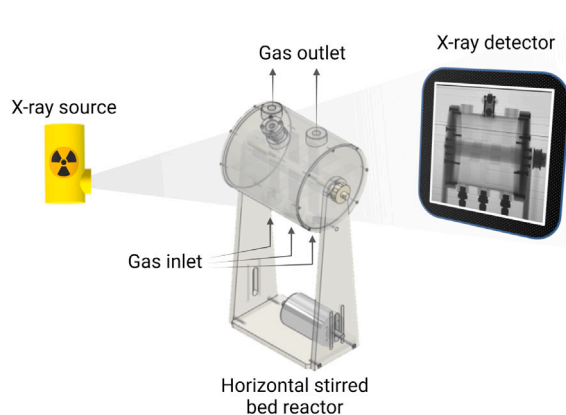


(a) Volume-based cumulative particle size distribution acquired with the Malvern 3000 particle size analyzer.

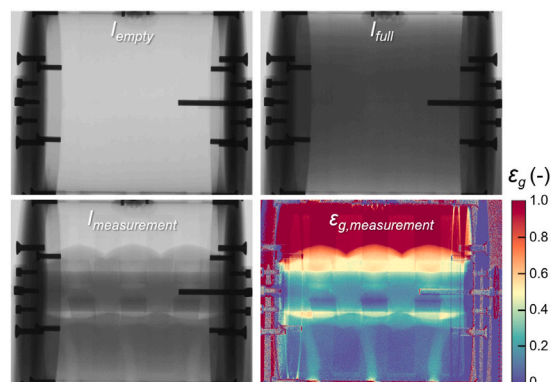


(b) Representative examples of optical microscope images of PP-1 (1) and PP-3 (2) and scanning electron microscope images of PP-1 (3) and PP-3 (4).

Fig. 3. Properties of the PP reactor powders used in this study.



(a) Schematic representation of the experimental setup.



(b) A two-point calibration procedure is employed to convert the intensity map to a gas holdup map.

Fig. 4. X-ray imaging analysis of the horizontal stirred bed reactor hydrodynamics.

the measurement intensity map ($I_{\text{measurement}}$) using the empty and full reference as depicted in Fig. 4(b). The normalized gas holdup ϵ_g was calculated as follows:

$$\epsilon_g = \frac{\ln(I_{\text{measurement}}/I_{\text{full}})}{\ln(I_{\text{empty}}/I_{\text{full}})} \quad (2)$$

It is important to note that the normalized gas holdup in this study ranges from 0 to 1, where 1 represents pure gas and 0 dense packing of solids. Warm colors in the gas holdup map correspond to low X-ray attenuation, indicating high gas concentrations. In contrast, cold colors represent high X-ray attenuation, indicating low gas concentrations. A more detailed description of the procedure is included in our previous works [33,34].

2.3. Operation and flow characterization

During the operation of the HSBR in industrial applications, the bed level is kept at constant inventory, and the rotation speed and gas inlet flow rate are kept constant. Adequate control of the operating settings is necessary to prevent operational issues, as these have a significant influence on the flow pattern in rotating systems [24,35]. This study evaluates the impact of agitation, gas inlet, and liquid content on the flow behavior of the PP powders in the laboratory-scale HSBR.

Three different types of experiments were conducted to elucidate the flow behavior of the PP reactor powders in the HSBR. In the first set

of experiments, the gas holdup was studied as a function of the rotation speed and gas inlet flow rate. The second set of experiments focused on determining how rotation speed and gas inlet flow rate affect the power consumption of the motor during agitation. Finally, the third set of experiments investigated the influence of liquid content on the flowability of the PP reactor powders.

For each experiment, the HSBR was filled to the desired level by inserting PP powder through the top opening. Depending on the specific experiment, either the gas inlet was activated or the IPA liquid was introduced. The agitator rotation speed was then set to the desired value. After 30 s, the X-ray source and detector were switched on, and X-ray images were acquired for a measurement duration of 60 s at varying acquisition frequencies. For the gas holdup experiments, the gas holdup was computed from the X-ray images according to the processing workflow described in Section 2.2.1. The operational settings are summarized in Table 2, and the different types of experiments will be discussed in more detail in the subsequent subsections.

2.3.1. Gas holdup

In the Innovene™ process, propylene gas is inserted through gas inlet openings at the bottom of the HSBR. In this cold model study, compressed air was supplied to the HSBR through three gas inlet points at the bottom positioned at 25, 50, and 75% of the reactor length. To assess the influence of the inlet flow rate on the gas holdup, the

Table 2
Experimental investigations and their respective operational settings.

Parameter	Gas holdup	Power consumption	Wet flow behavior
Fill level (v%)	50	50	50
Rotation speed (RPM)	20-40-60	20-40-60	20-40-60
Total gas inlet (L min ⁻¹)	0-15-30-45-60	0-30-60	0
Liquid content (vol%)	0	0	0.00-1.25-2.50-5.00-10.0
Sampling frequency X-ray (Hz)	35-70	RPM dependent	35
Measurement run time (s)	60	60	60

flow rate was incrementally increased from 0 to 60 L min⁻¹ in steps of 15 L min⁻¹ for various rotation speeds.

The gas holdup of the entire HSBR was acquired with an X-ray acquisition frequency of 35 Hz. To capture the fast dynamics of the gas holdup directly above the gas inlet, the gas holdup of the bottom half of the HSBR was acquired with an X-ray acquisition frequency of 70 Hz. The time-resolved X-ray images could be converted to time-averaged gas holdup by averaging the intensity of the captured X-ray images during the 60 s acquisition time and subsequently applying the two-point calibration protocol described in Section 2.2.1.

2.3.2. Power consumption

Monitoring the power consumption of the motor under the influence of varying rotation speeds (20, 40, and 60 RPM) and varying inlet flow rates (0, 30, and 60 L min⁻¹) during agitation gives valuable insight in the variation of the resistance. To monitor the power consumption, in-house integrated logging software in LabVIEW was used. During agitation, the software automatically logged the current of the motor at a specific arbitrary agitator position, ranging from 0 to 4096 during one revolution. The logged current and position were stored for further data processing. The arbitrary current was converted to power by employing a calibration protocol, and the arbitrary agitator position was converted to the angle of rotation with Eq. (3).

$$\text{Angle of rotation} = \frac{\text{Position number}}{4096} \cdot 360 \quad (3)$$

To understand how the power consumption of the motor relates to the gas holdup, X-ray images were captured at fixed agitator positions. This was achieved by incorporating the control of the X-ray apparatus into the power consumption logging software, which allowed the triggering of the X-ray detector at fixed agitator positions. Consequently, the sampling frequency of the X-ray detector depended on the number of positions and the rotation speed of the agitator. An in-depth analysis of the correlation between phase holdup and power consumption was made possible by capturing X-ray images while simultaneously logging the power consumption at the same agitator positions.

Additionally, by capturing X-ray images at identical agitator positions over a large number of revolutions, phase-locking the position, the consistency of the phase holdup could be analyzed. An in-house MATLAB script was used to compute the structural similarity index (SSIM) of the acquired X-ray images using the image acquired during the first revolution as a reference. The SSIM represents the similarity between two images, for which a value closer to 1 indicates a better similarity [36], and thereby allows quantitative assessment of the consistency of the phase holdup.

2.3.3. Wet flow behavior

In the Innovene™ PP process, a liquid propylene quench is used to remove heat originating from the exothermic polymerization reaction through evaporative cooling. Excessive quench liquid may cause the formation of agglomerates or lumps due to liquid bridge formation, which can adversely affect reactor efficiency. Furthermore, ensuring sufficient solids motion is essential for achieving uniform liquid distribution. Therefore, it is crucial to quantify the influence of the liquid content and rotation speed on the flowability of PP reactor powder.

As propylene is in a gaseous state under standard temperature and pressure conditions, isopropyl alcohol (IPA) was used as a model liquid.

Measurements were conducted with fixed liquid contents of 0.00, 1.25, 2.50, 5.00, and 10.0 vol% IPA by adding IPA through the top opening and agitating for 30 s to ensure a homogeneous mixture. For each liquid content, X-ray images of the flow behavior in the HSBR were captured at rotation speeds of 20, 40, and 60 RPM.

Besides a qualitative assessment of the flow behavior under various liquid contents, the deviation of the flow pattern from the normal flow pattern (0 vol% at 20 RPM) was quantitatively assessed based on the variation of the surface position. Typically, a consistent flowing surface with a low degree of variation corresponds to a good flowability, while an irregular flowing surface with a high degree of variation corresponds to a poor flowability [37]. Using this characteristic, an in-house MATLAB script was employed to compute a time-averaged X-ray image for each operational setting. Then, for each time-averaged image, the top part of the bed was extracted, and the SSIM was computed using the time-averaged X-ray image acquired under dry conditions (0 vol% IPA) at a rotation speed of 20 RPM as a reference, representing the normal flow behavior. As depicted in the previous section, the SSIM represents the similarity between two images, for which a value closer to 1 indicates a better similarity. In this way, the SSIM allows quantitative assessment of the deviation from the normal flow pattern when the bed is exposed to various liquid contents.

3. Results and discussion

3.1. Gas holdup

3.1.1. Gas holdup without gas inlet

A significant advantage of the employed X-ray imaging method is its ability to offer a direct projection of the gas holdup over time, enabling the visualization of both time-resolved and time-averaged flow behavior and gas holdup. Fig. 5(a) presents the time-averaged gas holdup without gas inlet, facilitating a qualitative comparison of the observed flow behavior of the two PP powders at different rotation speeds.

It can be observed that the clockwise impeller rotation causes the left side of the bed to rise upward and flow over the shaft. A comparison of different rotation speeds reveals that the bed expands as rotation speed increases. The expansion is attributed to the aeration of the bed due to the fast rotation of the impeller blades, which brings the bed to an aerated state. The phenomenon of aeration at elevated rotation speeds is commonly observed in rotating drums, especially for fine powders [38].

The aeration of the bed is also observed by closely evaluating the gas holdup at the different rotation speeds. As the rotation speed increases, both PP powders demonstrate a gradual increase in gas holdup. This increase is particularly noticeable at the left and upper regions of the bed, visually depicted by a lighter blue shade, indicative of a more aerated and loosely packed state. This observation is graphically reinforced by the vertical line profile in Fig. 5(b), which shows that a higher gas holdup is attained at a higher rotation speed. Additionally, both the spatial gas holdup maps (Fig. 5(a)) and the vertical profiles (Fig. 5(b)) highlight that PP-3 remains a slightly higher gas holdup. Interestingly, a region with lower gas holdup, depicted by a darker blue shade, is observed at the bottom right part of the bed in all instances, indicating a denser state. The region with a dense state is most likely

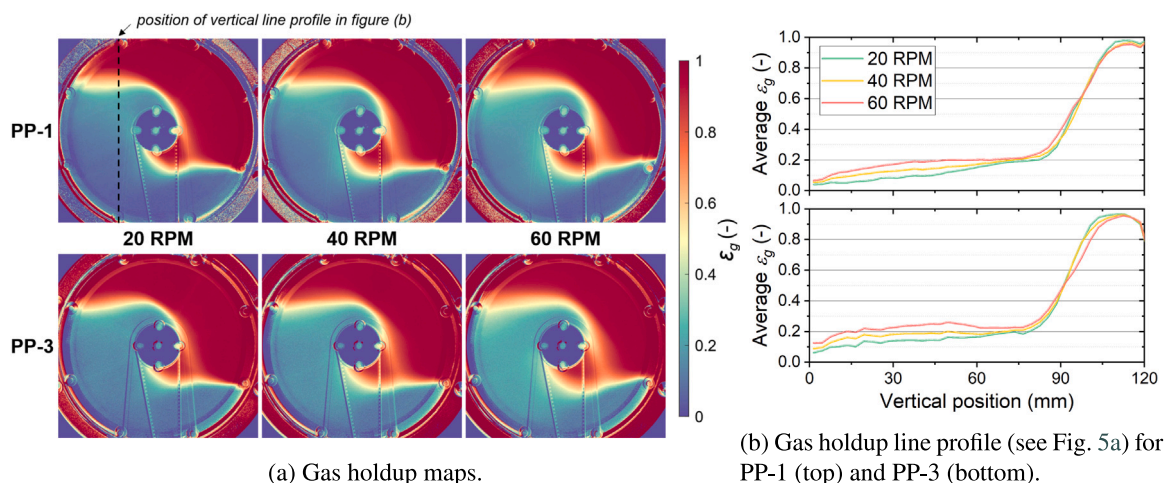


Fig. 5. Time-averaged gas holdup without gas inlet for various rotation speeds. A video displaying the time-resolved flow behavior is included in the electronic appendix.

caused by the compaction of the bed when the particles descend after flowing over the shaft.

The agitation-induced bed aeration leads to a rise in the material flow over the shaft, as evidenced by the time-averaged gas holdup. The circumferential motion of solids, driven by the clockwise agitation that compels material to flow over the shaft, plays a crucial role in achieving a well-mixed system with a uniform particle cycle time, as was reported by van der Sande et al. [26]. Comparing the gas holdup of the two PP powders across different rotation speeds reveals no significant differences. Both powders display free-flowing behavior and increased aeration with higher rotation speeds.

3.1.2. Gas holdup with gas inlet

In the industrial process, propylene gas is inserted through inlets spaced along the various polymerization sections of the HSBR and located underneath the surface of the polymer bed [7]. In this cold model study, compressed air was supplied to the HSBR through three gas inlet points at the bottom positioned at 25, 50, and 75% of the reactor length. Fig. 6 illustrates the gas holdup at various gas inlet flow rates for PP-1 (Fig. 6(a)) and PP-3 (Fig. 6(b)) for a rotation speed of 20 RPM.

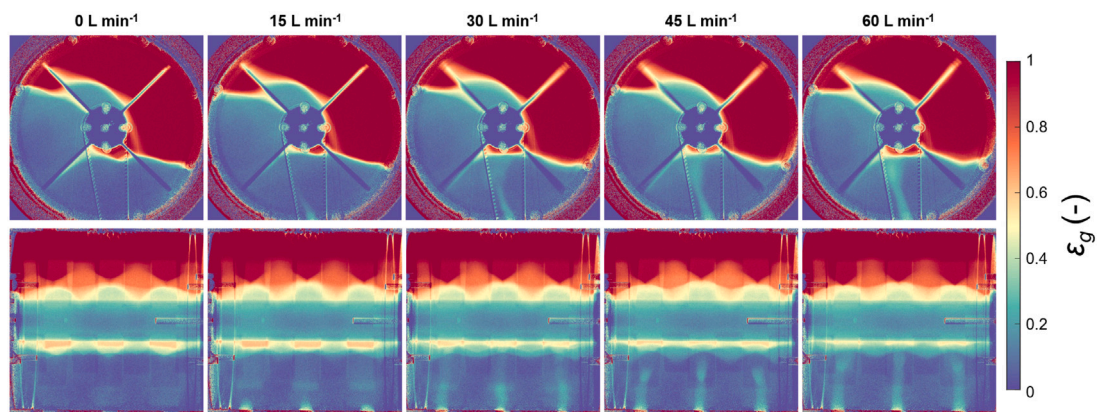
From both the front and side view, it is evident that gas spouts, characterized by a moderate gas holdup, are formed above the gas inlet points. These spouts increase in height with higher gas flow rates. From the front view, it can be observed that the spouts are formed at each gas inlet point, at 25, 50, and 75% of the reactor length. For PP-1, gas spouts begin developing at a gas flow rate of 15 L min^{-1} and bypass the bed (i.e., reaching up to the bed surface) from 30 L min^{-1} onwards. With PP-3 having a slightly higher u_{mf} than PP-1 (25 cm s^{-1} compared to 15 cm s^{-1}), gas spouts only form at a gas flow rate of 30 L min^{-1} and bypass the bed starting from 60 L min^{-1} .

Spouting is inherently linked to reduced gas–solid contacting, particularly in cases of complete bypass. In the industrial process, both gaseous propylene and hydrogen are introduced from the bottom of the HSBR. Since the HSBR operates under a propylene atmosphere, there is readily good contact between propylene gas and the solid phase, and the bypass of propylene is not expected to significantly affect the overall process efficiency. However, hydrogen plays a crucial role in controlling chain length and terminating the polymerization reaction, which requires effective gas–solid contact. Therefore, the bypass of hydrogen gas due to spouting is undesirable. Furthermore, the formation of spouts may locally induce solids circulation, as typically observed in the annulus region of spouted beds [39]. However, characterizing the motion of individual particles in the HSBR requires particle tracking methods, which are not the focus of this study but could serve as an extension for future investigations.

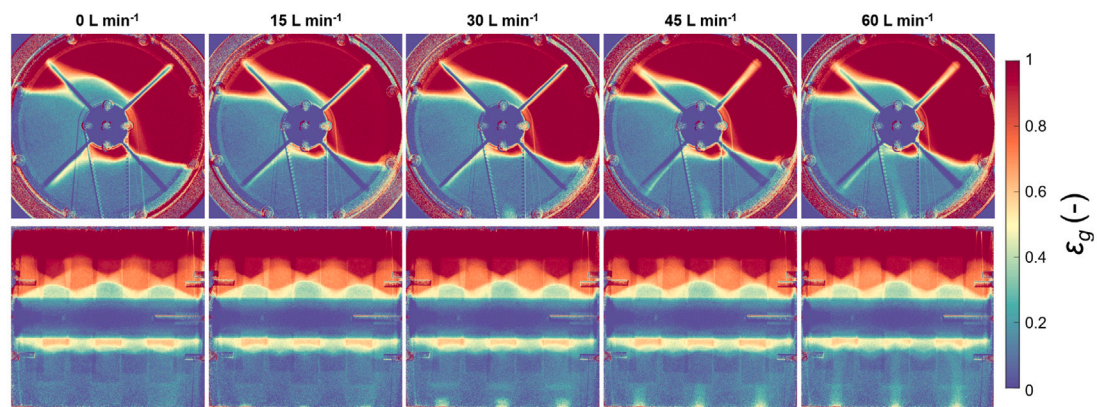
Upon close examination of the front-view gas holdup maps, the stark contrast in gas holdup between the spout and the surrounding bulk for both powders indicates limited axial mixing of gas within the solids phase. In the side-view gas holdup maps, the influence of clockwise agitation on the spout's trajectory is evident, with the spout bending toward the left side of the bed. This observation suggests tangential mixing of gas within the solids phase due to the rotational movement of the impeller blades, underscoring the significant role of agitation in the gas distribution. To further elucidate the agitation's influence on the gas inlet dynamics, Fig. 7 presents sequences of snapshots of the time-resolved gas holdup, acquired with an X-ray image acquisition frequency of 70 Hz, at a rotation speed of 20 RPM and gas flow rates of 15 and 60 L min^{-1} for one-quarter of the agitator revolution, corresponding to a time period of 0.75 s.

The first snapshot ($t=0.0 \text{ s}$) illustrates the gas holdup when three impeller blades (see Fig. 2 and the description of the HSBR geometry) align with the gas injection points. For powder PP-1, gas spouts are clearly observed right of the downward-facing impeller blades at both gas flow rates. Conversely, for PP-3, a clear gas spout is formed at a flow rate of 60 L min^{-1} while a minor gas spout is observed at a flow rate of 15 L min^{-1} , which is in agreement with previous observations made from Fig. 6(b). From the next snapshot ($t=0.19 \text{ s}$), it can be observed that the formed gas spouts bend toward the wakes behind the passing impeller blades, following the clockwise movement of the agitator. In the third snapshot ($t=0.38 \text{ s}$), the gas inlet is positioned between the passing blade and the approaching blade. For both powders, it can be observed that at a flow rate of 60 L min^{-1} , the spouts remain directed toward the impeller, while at 15 L min^{-1} , it diverges from the passing impeller blades. Subsequent to this ($t=0.56 \text{ s}$), a significant reduction of the spouts is observed for PP-1 at a flow rate of 15 L min^{-1} and PP-3 at a flow rate of 60 L min^{-1} , while it continues to be fully developed for PP-1 at a flow rate of 60 L min^{-1} . This reduction is attributed to the approaching impeller blades pushing the powder toward the gas inlet. Finally, the last snapshot ($t=0.75 \text{ s}$) captures the gas holdup when four impeller blades align with the gas injection points. The impeller blades offer a path of lesser resistance, leading to the reformation of spouts for PP-1 at 15 L min^{-1} and PP-3 at 60 L min^{-1} . This analysis underscores the significant influence of agitation on gas holdup dynamics.

It should be noted, however, that gas injection into the bed does not significantly impact the overall hydrodynamics of the bed. Comparing gas holdup maps obtained at flow rates of 0 L min^{-1} and 60 L min^{-1} (see Fig. 5), only minor bed surface restructuring due to slight bed expansion is evident. Apart from this minimal surface restructuring, the overall bed dynamics remain largely consistent across varying gas inlet flow rates. As previously mentioned, agitation appears to be the dominant factor influencing flow behavior.

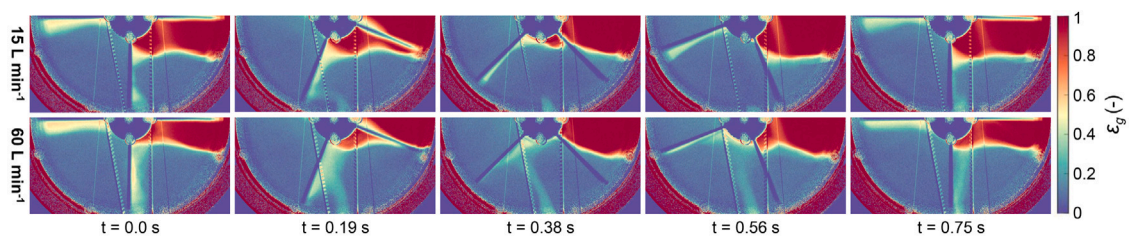


(a) Powder PP-1.

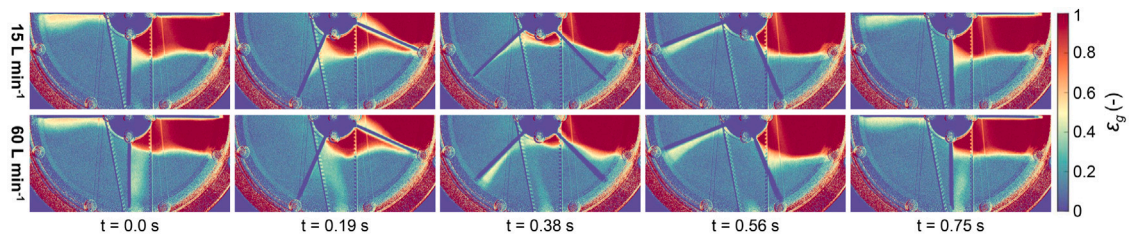


(b) Powder PP-3.

Fig. 6. Representative gas holdup snapshots for varying gas flow rates at a rotation speed of 20 RPM displaying the side and front view of the HSRB.

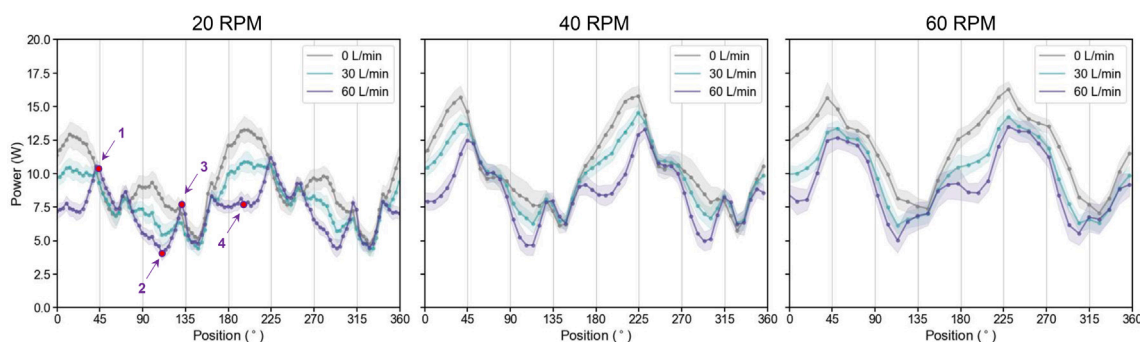


(a) Powder PP-1.

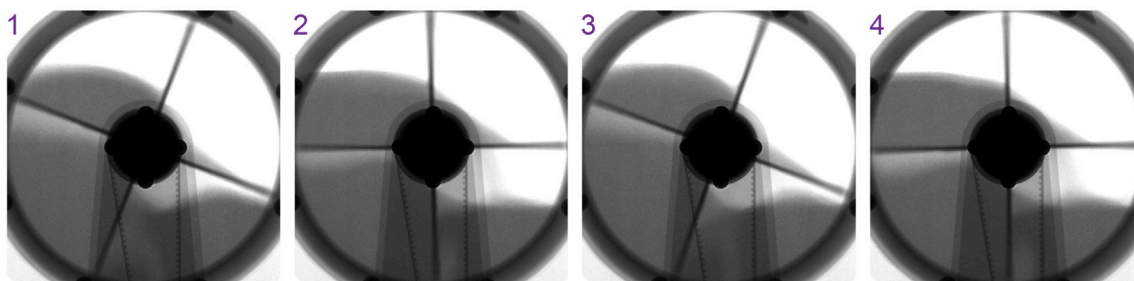


(b) Powder PP-3.

Fig. 7. Time sequence of representative gas holdup snapshots of the bottom half of the HSRB acquired at a rotation speed of 20 RPM and a flow rate of 15 and 60 L min⁻¹. This sequence chronologically (from left to right) depicts gas holdup dynamics under the influence of the clockwise movement of the impellers through the bed during a 0.75 s time period.



(a) Graphical representation of the power consumption fluctuations within one revolution for powder PP-3 for varying rotation speed (20, 40, and 60 RPM) and gas inlet flow rate (0, 30, and 60 L min⁻¹). The mean and standard deviation are based on 60 revolutions.



(b) X-ray images acquired at a rotation speed of 20 RPM and inlet flow rate of 60 L min⁻¹ corresponding to the numbered positions indicated in Fig. 8a.

Fig. 8. The influence of the agitation and gas inlet flow rate on the power consumption within one revolution for powder PP-3. A video demonstrating the evolution of power consumption during a revolution is included in the electronic supplementary.

3.2. Power consumption

In the preceding section, we explored the effects of rotation speed and gas inlet flow rate on gas holdup within the HSBR. It was demonstrated that higher rotation speeds induce mechanical aeration of the powder bed, while gas inlet can lead to spouting behavior. In this section, we broaden our investigation to include the influence of rotation speed and gas inlet flow rate on the power consumption of the motor. Utilizing an integrated phase-locking method, as described in Section 2.3.2, we obtained time-resolved power consumption data during agitator revolutions.

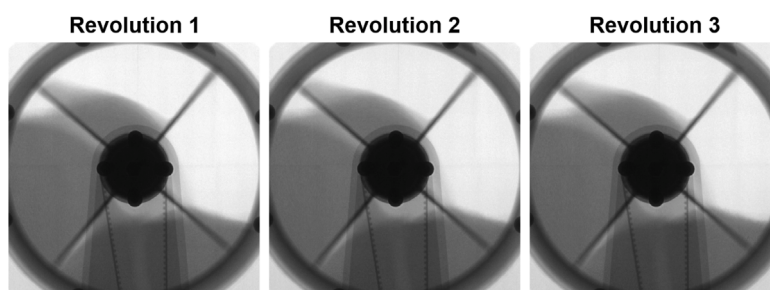
Fig. 8(a) illustrates the power consumption within one revolution (i.e., 0 to 360°) for powder PP-3 at varying rotation speeds and gas inlet flow rates. The graphs notably depict an oscillating pattern, indicating fluctuating power consumption throughout a single agitator revolution. In the case of 0 L min⁻¹ gas inlet (the gray lines in Fig. 8(a)), this oscillating pattern can be attributed to two factors. Firstly, during agitation, the powder is pushed upward in a clockwise manner until it freely flows over the shaft downward. It is evident that the impellers require more power to push the powder upward, as gravity opposes this movement, compared to moving through air. The peaks in the graph correspond to moments when an impeller blade transitions from air into the powder bed, resulting in apparent stick-slip behavior. Stick-slip behavior, extensively studied by researchers such as Albert et al. [40], commonly arises from external stress applied to granular media, causing an internal structure that resists the stress and leads to a jammed state. As the impeller blade's motion is impeded by jammed particles ahead of it, when the applied force surpasses a critical threshold, the blade advances further into the powder bed, displacing the particles.

Secondly, the geometry of the agitator contributes to the observed oscillating pattern. The agitator comprises a shaft with seven axial

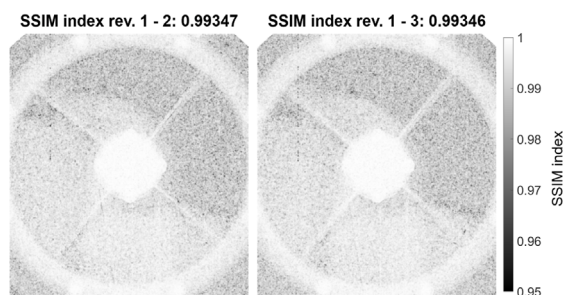
blade positions, each equipped with two blades positioned 90° apart from neighboring blades. This uneven distribution of blades results in a variation in total blade surface area within the bed during the clockwise rotation of the agitator, leading to varying resistance. Consequently, this variance contributes to differences in power consumption values at the peaks. The relatively large difference is due to the limited number of blade positions in the laboratory-scale HSBR, namely 7. In industrial HSBRs, where the number of blade positions is significantly larger, the influence of uneven blade distribution is expected to be considerably smaller. Interestingly, a detailed examination of the graphs reveals that the oscillating pattern repeats every 180°, which is attributed to the system's symmetry.

When gas is introduced into the system, as indicated by the turquoise and purple lines in Fig. 8(a), four distinct regions are observed where there is a notable deviation in power consumption compared to the 0 L min⁻¹ cases. These deviations occur when the impeller blades pass over the gas inlet. As demonstrated in the previous section, gas spouts form above the gas inlet points. When impeller blades traverse the gas spout, they encounter significantly less resistance compared to moving through the bed material. The deviation begins as the blades approach the gas inlet, reaches its maximum when the blades align with the gas inlet, and diminishes as the blades move away from the gas inlet.

Within one revolution, there are two instances when four blades traverse over the gas inlet, resulting in the most significant deviation from the 0 L min⁻¹ case (as indicated by Fig. 8 number 4). Similarly, there are two instances when three impeller blades move over the gas inlet, resulting in a smaller deviation from the 0 L min⁻¹ case (as indicated by Fig. 8 number 2). The disparity in deviation of power consumption relative to the 0 L min⁻¹ case stems from the larger total blade surface area of four blades compared to three blades. This observation underscores the influence of the gas inlet on motor power



(a) Sequence of X-ray images captured at identical agitator positions for succeeding revolutions.



(b) Structural similarity index (SSIM) demonstrating the similarity between Fig. 9a images 1 and 2 (left) and images 1 and 3 (right).

Fig. 9. Similarity between X-ray images acquired at identical agitator positions a rotation speed of 20 RPM and a gas flow rate of $60\text{ L}\cdot\text{min}^{-1}$.

consumption. As observed for the $0\text{ L}\cdot\text{min}^{-1}$ cases, it can also be noted that the patterns with gas inlet repetition occur every 180° due to symmetry in the system.

Comparing the graphs obtained at different rotation speeds, it becomes evident that the 20 RPM graphs exhibit a minimum of four peaks, varying in power value due to the agitator configuration, as previously explained. Interestingly, the peaks with lower power consumption are nearly absent in the 40 RPM graphs and completely absent in the 60 RPM graphs. As established in the previous section, an increase in rotation speed leads to mechanical bed aeration. Apart from reducing local bulk density, aeration can mitigate stick-slip behavior, resulting in smoother power consumption during agitation [41]. Consequently, this reduction in stick-slip behavior leads to a decrease in the number of peaks in the graph.

The power consumption of PP-1 exhibits a comparable oscillating pattern during agitation, as shown in supplementary Fig. C.1. However, a noticeable difference between the two PP reactor powders is that PP-1 requires an overall higher power consumption, with oscillations having a larger amplitude at similar operational settings. This disparity in power consumption and amplitude between PP-1 and PP-3 can be attributed to the higher bulk density of PP-1. Since experiments were conducted using a consistent volume of PP reactor powder, the bed constituted a higher mass during experiments with PP-1 compared to PP-3. Consequently, more power is required for the agitation of PP-1. These findings align with those of Knight et al. [42], who investigated the impact of mass on power consumption in high-shear powder mixers and concluded that power consumption increases with higher agitated mass. Similar to PP-3, the degree of variation in power consumption is reduced with increasing rotation speed, attributed to the aeration of the bed.

Despite the system's multiphase and discrete nature, remarkably small standard deviations are observed at each agitator position in Fig. 8(a) and supplementary Fig. C.1, indicating highly consistent behavior. To further illustrate the bed's consistency, Fig. 9(a) presents a sequence of three X-ray images acquired at identical agitator positions for successive revolutions obtained through the X-ray imaging integrated phase-locking method.

Upon qualitative comparison of the images with the naked eye, no discernible differences can be observed. To further quantify their similarity, the structural similarity index (SSIM) was computed using image revolution 1 as the reference. As explained in Section 2.3.2, the SSIM represents the similarity between two images, with a value closer to 1 indicating better similarity. The SSIM index maps, depicted in Fig. 9(b), along with the global SSIM index values of 0.99347 (image revolution 2) and 0.99346 (image revolution 3), indicate extremely high similarity. In fact, the primary difference between the images lies in the noise present in the high-intensity regions of the image (where there is no powder or flange). This suggests that the bed and gas spout exhibit remarkable consistency across successive revolutions. Since the images are acquired at identical agitator positions, it further underscores that both the bed behavior and gas spout behavior are predominantly influenced by agitation. These findings are significant, as the bed's extremely high consistency implies that the system can be reliably characterized within a short measurement time. This is particularly relevant for computational modeling, such as Computational Fluid Dynamics-Discrete Element Modeling (CFD-DEM). Such modeling is highly CPU demanding, and investigations are therefore limited to short duration. The recurrent patterns in the HSBR open doors to the employment recurrence CFD approaches [43], potentially speeding up the simulations by two orders of magnitude [44].

3.3. Flowability under wetted conditions

In the preceding sections, we explored the impact of rotation speed and gas inlet flow rate on gas holdup in the HSBR under dry conditions. However, in the industrial polymerization process, the bed is continuously wetted by a propylene quench to dissipate heat generated by the exothermic polymerization reaction. In this section, we investigate the effect of liquid on the flow behavior in the HSBR by subjecting the PP reactor powders to various IPA contents. Fig. 10 presents representative snapshots illustrating the flow behavior of the two PP reactor powders across IPA liquid contents ranging from 0 to 10 vol%.

Under dry conditions (0.00 vol%), both powders exhibit a smooth flowing layer, indicative of good flowability. However, notable differences in flow behavior emerge upon exposure to IPA. While PP-3

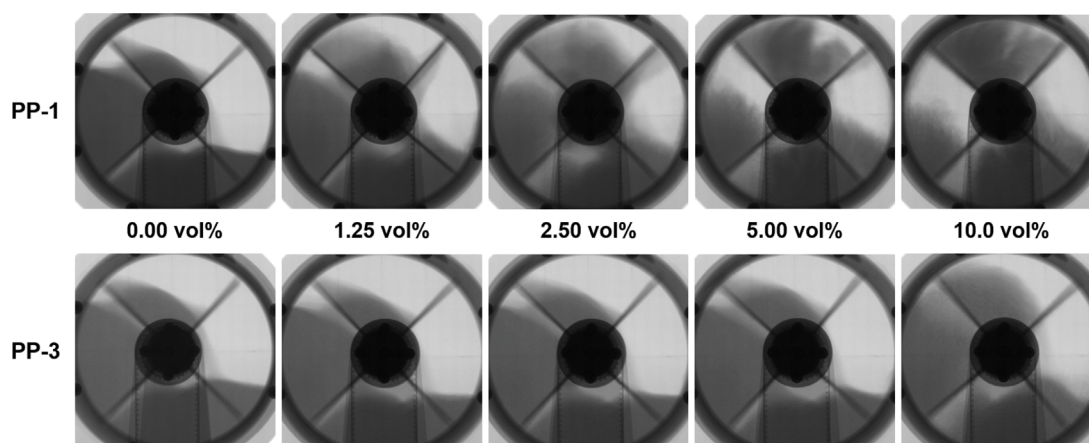


Fig. 10. Representative X-ray images of the flow behavior of PP-1 (top) and PP-3 (bottom) at a rotation speed of 20 RPM for liquid contents of 0, 1.25, 2.50, 5.00, and 10 vol% isopropyl alcohol. A video of the flow behavior is included in the electronic supplementary.

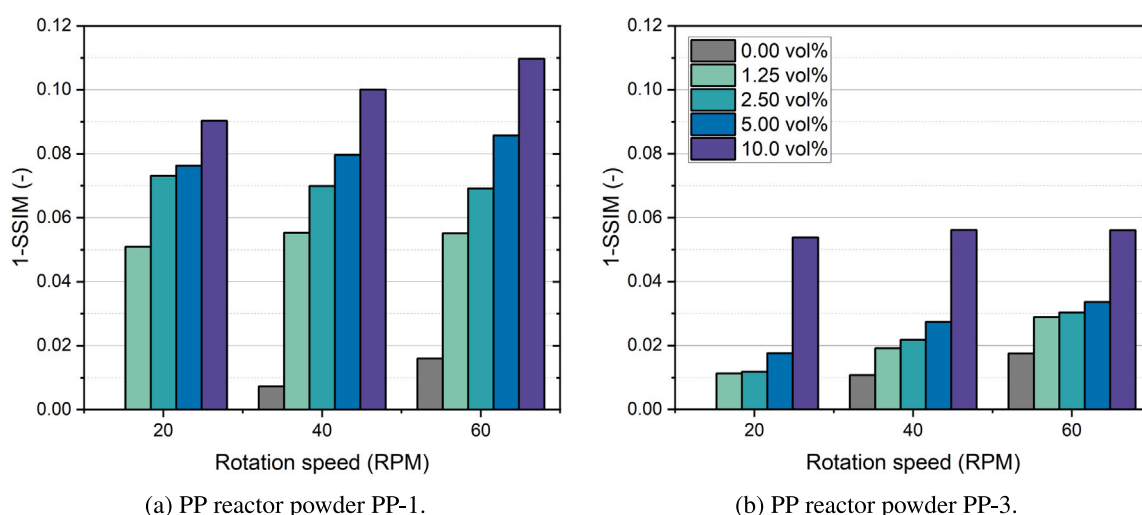


Fig. 11. The influence of liquid content and rotation speed on the deviation in flow pattern (1-SSIM) relative to the flow pattern acquired under dry conditions at a rotation speed of 20 RPM.

maintains a smooth flowing layer for liquid contents up to 5.00 vol%, PP-1 demonstrates deteriorated flowability already at a liquid content of 1.25 vol%, evidenced by an irregular flowing layer. The deterioration of flowability persists with increasing liquid content. Eventually, at a liquid content of 10 vol%, cohesive forces become so pronounced that lumps of PP cycle circumferentially, rendering the powder no longer flowing. Although PP-3 also experiences a reduction in flowability at a liquid content of 10.00 vol%, it remains significantly more flowable than PP-1.

An image processing workflow was employed to quantify the deviation in flow patterns under wetted conditions. For each operational condition, the SSIM of the time-averaged flow pattern was computed with the time-averaged flow pattern acquired at 20 RPM under dry conditions serving as the reference. As previously mentioned, the SSIM represents the similarity between two images, with a value closer to 1 indicating better similarity. Utilizing the flow behavior under dry conditions at a rotation speed of 20 RPM as a reference, the value of 1-SSIM represents the deviation in the flow pattern from the normal flow behavior at 20 RPM. Consequently, a larger value for 1-SSIM indicates a greater deviation. Fig. 11 graphically illustrates the influence of liquid content and rotation speed on the deviation in flow pattern from the flow pattern under dry conditions at a rotation speed of 20 RPM.

In agreement with Fig. 5, it can be observed that increasing the rotation speed results in a small deviation in the flow pattern, which is

attributed to the aeration of the bed. More interestingly, by comparing the influence of the liquid content for both powders, significant differences in the deviation of the flow pattern are observed. As qualitatively depicted in 5, Fig. 11(a) illustrates that the flow pattern of PP-1 already exhibits significant deviation from the normal flow pattern at a liquid content of 1.25 vol% and continues to deviate up to a 1-SSIM value of 0.11 at a liquid content of 10 vol% for a rotation speed of 60 RPM. In contrast, Fig. 11(b) demonstrates that the flow pattern of PP-3 only begins to deviate significantly at a liquid content of 10.0 vol%. Remarkably, the deviation in the flow pattern of PP-3 at 10.0 vol% is comparable to the deviation in the flow pattern of PP-1 at 1.25 vol%, underscoring the substantial difference in susceptibility to liquid between the two PP reactor powders.

The observed differences in the apparent impact of liquid content on the flowability of the two PP reactor powders can be elucidated by their distinct particle properties. As discussed in Section 2.2, PP-1 has a Sauter mean diameter of 569 μm and comprises angular-shaped particles with a dense surface, whereas PP-3 possesses a Sauter mean diameter of 1040 μm and comprises spherical-shaped particles with a porous surface. Both differences in particle size and particle surface may contribute to the observed disparity in flowability. When liquid droplets encounter the dense surface of PP-1 (refer to Fig. 3(b)-c), the liquid is readily present at the surface, forming liquid bridges at the contact points between particles. This process enhances the cohesiveness of the powder, even at low liquid contents. Conversely, the porous

surface of PP-3 (refer to Fig. 3(b)-d) allows liquid to permeate into the pores. Here, the absorbed liquid is not readily available at the surface to form liquid bridges, thereby exerting minimal influence on cohesion. Only when the pores become saturated does the IPA become available at the surface, resulting in liquid bridging that gradually enhances cohesiveness. These results underscore the importance of considering the properties of the polymerized product in the industrial HSBR when tailoring process characteristics.

4. Conclusions

In this study, the flow behavior of polypropylene (PP) reactor powder in a laboratory-scale horizontal stirred bed reactor (HSBR) was investigated using X-ray imaging. The influence of the agitator rotation speed, gas inlet flowrate, and liquid content on the flow behavior and phase holdup was evaluated, yielding the following conclusions:

- The overall flow behavior and phase holdup in the HSBR are strongly dictated by the agitation with the stirrer. Operation at increased rotation speed results in aeration of the bed, which in turn results in an increase in the mass flow of PP powder over the shaft.
- Gas injection through the inlet points at the bottom of the HSBR results in spouting behavior, which is more dominant for reactor powder with a smaller particle size (PP-1) compared to the powder with a larger particle size (PP-3). Spouting behavior results in reduced gas–solid contacting and, in extreme cases, complete bypass, which will be disadvantageous for most applications.
- Agitation, as well as alternation of the impeller blade positions, influence the gas holdup and result in variations in power consumption within an agitator revolution. The degree of fluctuation in powder consumption decreases with increasing rotation speeds due to the aeration of the bed. The gas holdup at fixed agitator positions is extremely consistent for succeeding revolutions, underlining the dominance of the agitation on the overall flow behavior.
- The presence of liquid isopropyl alcohol deteriorates the flow behavior of the PP reactor powder. Liquid bridging at the contact points of particles results in a cohesive force that leads to the formation of lumps. The particle size and surface morphology highly influence the powders' susceptibility to liquid, as the flow behavior of PP powder with relatively small particle size and dense surface morphology is already strongly reduced at a liquid content of 1.25 vol%, while the flow behavior of the PP powder with larger particle size and porous surface is only reduced at a liquid content of 10 vol%.

The insights acquired from this work not only provide a further understanding of the flow behavior and phase holdup in HSBRs but can also serve as a valuable basis for optimizing, intensifying, and scaling HSBR systems for the manufacturing of high-quality PP resins on an industrial scale.

CRedit authorship contribution statement

P. Christian van der Sande: Writing – review & editing, Writing – original draft, Visualization, Validation, Software, Methodology, Investigation, Formal analysis, Data curation, Conceptualization. **Claris de Vries:** Writing – original draft, Investigation, Formal analysis, Data curation. **Evert C. Wagner:** Writing – review & editing, Software, Methodology, Investigation, Data curation, Conceptualization. **Amarenske C. Vögtlander:** Investigation, Formal analysis, Data curation. **Gabrie M.H. Meesters:** Writing – review & editing, Supervision, Project administration, Conceptualization. **J. Ruud van Ommen:** Writing – review & editing, Supervision, Project administration, Methodology, Funding acquisition.

Declaration of competing interest

The authors declare the following financial interests/personal relationships which may be considered as potential competing interests: J.R. van Ommen reports financial support was provided by Dutch Research Council. If there are other authors, they declare that they have no known competing financial interests or personal relationships that could have appeared to influence the work reported in this paper.

Acknowledgments

The authors would like to thank Stefan ten Hagen for his contribution to the development of the laboratory-scale HSBR. Moreover, they thank Hans van der Does and Rolf Kalbermatter for the development of the LABview logging software.

This work was carried out as part of the 'Industrial Dense Granular Flows' project, which received funding from the Dutch Research Council (NWO) in the framework of the ENW PPP Fund for the top-sectors and from the Ministry of Economic Affairs in the framework of the 'PPS-Toeslageregeling'.

Appendix A. Supplementary data

Supplementary material related to this article can be found online at <https://doi.org/10.1016/j.cej.2024.156891>.

Data availability

Data will be made available on request.

References

- [1] J. Karger-Kocsis, T. Bárány, *Polypropylene Handbook Morphology, Blends and Composites: Morphology, Blends and Composites*, 2019.
- [2] K. Kulajanpeng, N. Sheibat-Othman, W. Tanthapanichakoon, T.F.L. McKenna, Multiscale modelling of multizone gas phase propylene (co)polymerization reactors—A comprehensive review, *Can. J. Chem. Eng.* 100 (9) (2022) 2505–2545.
- [3] Statista, Market volume of polypropylene worldwide from 2015 to 2022, with a forecast for 2023 to 2030, 2023, URL: <https://www.statista.com/statistics/1245169/polypropylene-market-volume-worldwide/>. (Accessed 24 May 2024).
- [4] Insights, Fortune Business, Polypropylene Market Size, Share & Trends, Report, 2020, URL: <https://www.fortunebusinessinsights.com/industry-reports/polypropylene-pp-market-101583>.
- [5] J.J. Zacca, J.A. Debling, W.H. Ray, Reactor residence time distribution effects on the multistage polymerization of olefins—I. Basic principles and illustrative examples, polypropylene, *Chem. Eng. Sci.* 51 (21) (1996) 4859–4886.
- [6] J. Shepard, J. Jezl, E. Peters, R. Hall, Divided horizontal reactor for the vapor phase polymerization of monomers at different hydrogen levels, 1976, U.S. Patent 3 957 448, May.
- [7] J. Jezl, E. Peters, R. Hall, J. Shepard, Process for the vapor phase polymerization of monomers in a horizontal, quench-cooled, stirred-bed reactor using essentially total off-gas recycle and melt finishing, 1976, U.S. Patent 3 965 083, June.
- [8] M. Caracotsios, Theoretical modelling of Amoco's gas phase horizontal stirred bed reactor for the manufacturing of polypropylene resins, *Chem. Eng. Sci.* 47 (9) (1992) 2591–2596.
- [9] A.B. Gorbach, S.D. Naik, W.H. Ray, Dynamics and stability analysis of solid catalyzed gas-phase polymerization of olefins in continuous stirred bed reactors, *Chem. Eng. Sci.* 55 (20) (2000) 4461–4479.
- [10] C.J. Dittrich, S.M.P. Mutsers, On the residence time distribution in reactors with non-uniform velocity profiles: The horizontal stirred bed reactor for polypropylene production, *Chem. Eng. Sci.* 62 (21) (2007) 5777–5793.
- [11] R.A. Hutchinson, Modelling of Particle Growth in Heterogeneous Catalyzed Olefin Polymerization (Ph.D. thesis), University of Wisconsin-Madison, 1990.
- [12] J.R. van Ommen, M.-O. Coppens, C.M. van den Bleek, J.C. Schouten, Early warning of agglomeration in fluidized beds by attractor comparison, *AIChE J.* 46 (11) (2000) 2183–2197.
- [13] C. M. van den Bleek, M.-O. Coppens, J. C. Schouten, Application of chaos analysis to multiphase reactors, *Chem. Eng. Sci.* 57 (22) (2002) 4763–4778, Festschrift in Honour of Dr Winn van Swaaij.
- [14] J. Wang, Y. Cao, X. Jiang, Y. Yang, Agglomeration detection by acoustic emission (AE) sensors in fluidized beds, *Ind. Eng. Chem. Res.* 48 (2009).

- [15] J.N. Israelachvili, *Intermolecular and Surface Forces*, Academic Press, London ; San Diego, 1991.
- [16] R.A. Hutchinson, W.H. Ray, Polymerization of olefins through heterogeneous catalysis. VII. Particle ignition and extinction phenomena, *J. Appl. Polym. Sci.* 34 (2) (1987) 657–676.
- [17] N.P. Khare, B. Lucas, K.C. Seavey, Y.A. Liu, A. Sirohi, S. Ramanathan, S. Lingard, Y. Song, C.-C. Chen, Steady-state and dynamic modeling of gas-phase polypropylene processes using stirred-bed reactors, *Ind. Eng. Chem. Res.* 43 (4) (2004) 884–900.
- [18] Z. Tian, X.-P. Gu, L.-F. Feng, J.-P. Corriou, G.-H. Hu, Modeling and simulation of polypropylene particle size distribution in industrial horizontal stirred bed reactors, *J. Appl. Polym. Sci.* 125 (2012).
- [19] M.F. Atan, M. Hussain, R. Abbasi, K. M.J.H, M. Patah, *Advances in mathematical modeling of gas-phase olefin polymerization*, *Processes* 7 (2019) 67.
- [20] Y. Xi, Q. Chen, C. You, Flow characteristics of biomass particles in a horizontal stirred bed reactor: Part I. Experimental measurements of residence time distribution, *Powder Technol.* 269 (2015) 577–584.
- [21] Y. Xi, Q. Chen, C. You, Flow characteristics of biomass particles in a horizontal stirred bed reactor: Part II. Modeling studies on particle residence time distribution and axial mixing, *Powder Technol.* 269 (2015) 585–595.
- [22] B. Laurent, J. Bridgwater, D. Parker, Convection and segregation in a horizontal mixer, *Powder Technol.* 123 (1) (2002) 9–18.
- [23] B. Laurent, J. Bridgwater, Performance of single and six-bladed powder mixers, *Chem. Eng. Sci.* 57 (10) (2002) 1695–1709.
- [24] B.F. Laurent, J. Bridgwater, Influence of agitator design on powder flow, *Chem. Eng. Sci.* 57 (18) (2002) 3781–3793.
- [25] P.C. van der Sande, J. de Mooij, E.C. Wagner, G.M. Meesters, J.R. van Ommen, Single-photon emission radioactive particle tracking method for hydrodynamic evaluation of multi-phase flows, *Particuology* (2023) in press.
- [26] P.C. van der Sande, E.C. Wagner, J. de Mooij, G.M. Meesters, J.R. van Ommen, Particle dynamics in horizontal stirred bed reactors characterized by single-photon emission radioactive particle tracking, *Chem. Eng. J.* 482 (2024) 149100.
- [27] M. Errigo, P. Lettieri, M. Materazzi, X-ray imaging techniques for gas–solid fluidized beds: A technical review, *Particuology* (2023).
- [28] K. Wu, E. Wagner, O. Ochkkin-Koenig, M. Franck, D. Weis, G. Meesters, J.R. Van Ommen, Time-resolved X-ray study of assisted fluidization of cohesive micron powder: On the role of mechanical vibration, *Chem. Eng. J.* 470 (2023) 143936.
- [29] A. Helmi, E.C. Wagner, F. Gallucci, M. van Sint Annaland, J.R. van Ommen, R.F. Mudde, On the hydrodynamics of membrane assisted fluidized bed reactors using X-ray analysis, *Chem. Eng. Process. Process. Intensif.* 122 (2017) 508–522.
- [30] M. Biebler, F. Barthel, U. Hampel, Ultrafast X-ray computed tomography for the analysis of gas–solid fluidized beds, *Chem. Eng. J.* 189–190 (2012) 356–363.
- [31] J. Yates, D. Cheesman, P. Lettieri, D. Newton, X-ray analysis of fluidized beds and other multiphase systems, *KONA Powder Part. J.* 20 (2002) 133–143.
- [32] R.L. Carr, Evaluating flow properties of solids, *Chem. Eng. J.* 72 (1965) 163–168.
- [33] R. Kamphorst, P.C. van der Sande, K. Wu, E.C. Wagner, M.K. David, G.M. Meesters, J.R. van Ommen, The mechanism behind vibration assisted fluidization of cohesive micro-silica, *KONA Powder Part. J.* 41 (2024) 254–264.
- [34] K. Wu, R. Kamphorst, A. Bakker, J. Ford, E.C. Wagner, O. Ochkkin-Koenig, M. Franck, D. Weis, G.M. Meesters, J.R. van Ommen, Stirrer design for improving fluidization of cohesive powder: A time-resolved X-ray study, *Chem. Eng. Sci.* 294 (2024) 120069.
- [35] P.M. Portillo, A.U. Vanarase, A. Ingram, J.K. Seville, M.G. Ierapetritou, F.J. Muzzio, Investigation of the effect of impeller rotation rate, powder flow rate, and cohesion on powder flow behavior in a continuous blender using PEPT, *Chem. Eng. Sci.* 65 (21) (2010) 5658–5668.
- [36] D. Brunet, E.R. Vrscay, Z. Wang, On the mathematical properties of the structural similarity index, *IEEE Trans. Image Process.* 21 (4) (2012) 1488–1499.
- [37] P. Tegzes, R. Albert, M. Paskvan, A.L. Barabási, T. Vicsek, P. Schiffer, Liquid-induced transitions in granular media, *Phys. Rev. E* 60 (5) (1999) 5823–5826.
- [38] A. Castellanos, M. Sanchez, J. Valverde, The onset of fluidization for fine powders in rotating drums, *Mater. Phys. Mech.* 3 (2001) 57–62.
- [39] A. Benkrid, H.S. Caram, Solid flow in the annular region of a spouted bed, *AIChE J.* 35 (8) (1989) 1328–1336.
- [40] I. Albert, P. Tegzes, R. Albert, J.G. Sample, A.L. Barabási, T. Vicsek, B. Kahng, P. Schiffer, Stick-slip fluctuations in granular drag, *Phys. Rev. E* 64 (3) (2001) 9.
- [41] C.M. Oprüşan, B. Chiriac, V. Cârlescu, D.N. Olaru, Influence of the stiffness and the speed on the stick-slip process, *IOP Conf. Ser. Mater. Sci. Eng.* 997 (1) (2020) 012016.
- [42] P.C. Knight, J.P.K. Seville, A.B. Wellm, T. Instone, Prediction of impeller torque in high shear powder mixers, *Chem. Eng. Sci.* 56 (2001) 4457–4471.
- [43] T. Lichtenegger, S. Pirker, Recurrence CFD – A novel approach to simulate multiphase flows with strongly separated time scales, *Chem. Eng. Sci.* 153 (2016) 394–410.
- [44] T. Lichtenegger, E. Peters, J. Kuipers, S. Pirker, A recurrence CFD study of heat transfer in a fluidized bed, *Chem. Eng. Sci.* 172 (2017) 310–322.